

Research Paper

Nanoliposomes Co-Encapsulating CT Imaging Contrast Agent and Photosensitizer for Enhanced, Imaging Guided Photodynamic Therapy of Cancer

Hao Xu^{1,2}, Tymish Y. Ohulchansky¹, Artem Yakovliev¹, Roman Zinyuk¹, Jun Song¹, Liwei Liu¹, Junle Qu¹, Zhen Yuan²

1. Key Laboratory of Optoelectronic Devices and Systems of Ministry of Education and Guangdong Province, College of Optoelectronic Engineering, Shenzhen University, Shenzhen, Guangdong 518060, P.R. China
2. Bioimaging Core, Faculty of Health Sciences, University of Macau, Avenida da Universidade, Taipa, Macau SAR 999078, P.R. China

✉ Corresponding authors: T.Y.O. (tyo@szu.edu.cn), J. Q. (jlqu@szu.edu.cn) or to Y.Z. (zhenyuan@umac.mo)

© Ivyspring International Publisher. This is an open access article distributed under the terms of the Creative Commons Attribution (CC BY-NC) license (<https://creativecommons.org/licenses/by-nc/4.0/>). See <http://ivyspring.com/terms> for full terms and conditions.

Received: 2018.10.30; Accepted: 2019.01.08; Published: 2019.02.12

Abstract

Fluorescence (FL) and X-ray computed tomography (CT) imaging-guided photodynamic therapy (PDT) can provide a powerful theranostic tool to visualize, monitor, and treat cancer and other diseases with enhanced accuracy and efficacy.

Methods: In this study, clinically approved iodinated CT imaging contrast agent (CTIA) iodixanol and commercially available photosensitizer (PS) meso-tetrakis (4-sulphonatophenyl) porphine (TPPS₄) were co-encapsulated in biocompatible PEGylated nanoliposomes (NL) for enhanced anticancer PDT guided by bimodal (FL and CT) imaging.

Results: The NL co-encapsulation of iodixanol and TPPS₄ (LIT) lead to an increase in singlet oxygen generation by PS via the intraparticle heavy-atom (iodine) effect on PS molecules, as it was confirmed by both direct and indirect measurements of singlet oxygen production. The confocal imaging and PDT of cancer cells were performed *in vitro*, exhibiting the cellular uptake of TPPS₄ formulations and enhanced PDT efficacy of LIT. Meanwhile, bimodal (FL and CT) imaging was also conducted with tumor-bearing mice and the imaging results manifested high-efficient accumulation and retention of LIT in tumors. Moreover, PDT of tumor *in vivo* was shown to be drastically more efficient with LIT than with other formulations of TPPS₄.

Conclusion: This study demonstrated that LIT can serve as a highly efficient theranostic nanoplatform for enhanced anticancer PDT guided by bimodal (FL and CT) imaging.

Key words: liposome, computed tomography, fluorescence bioimaging, photodynamic therapy, heavy atom effect

Introduction

A combination of diagnostics (i.e., imaging) and treatment modalities in a single formulation is essential to establish a theranostic platform for imaging-guided photodynamic therapy (PDT) [1-6]. In PDT, light of a specific wavelength is used to activate PDT drugs (photosensitizer, PS), which are non-toxic without light, enabling them to generate reactive oxygen species (ROS) that target and eradicate malignant cells and tissues [7]. The inherent

dual selectivity of PDT (i.e., localization of both light and PS at the diseased sites) enables a more precise spatiotemporal control of the noninvasive therapeutic action, as compared to that from other categories of treatment, such as chemotherapy and radiation [8]. Imaging-guided PDT is emerging as a prospective cancer treatment modality [1], allowing for the assessment of PS biodistribution including tumor delivery and uptake as well as body clearance [9]. In

this regard, a fluorescent PS can serve as both a contrast agent in fluorescence imaging (FLI) and as a PDT agent, providing basis for FLI-guided PDT [10]. However, the downside of FLI is that it can only provide information about the superficial tissues [11], which hampers its potential application in imaging guided PDT.

On the other hand, X-ray computed tomography (CT) imaging is one of the most reliable medical imaging techniques, which is extensively used in clinics. It provides a powerful diagnostic tool, allowing for deep tissue or whole-body imaging and offering a high spatial resolution and capability of three-dimensional (3D) visualization of biological tissues with short imaging time [12]. The spatio-temporal CT scanners are constantly being improved owing to increased numbers of new detectors. When administered, clinical agents that efficiently absorb X-rays can strongly increase the CT imaging contrast at regions of interest.

A complementary combination of high spatial-resolution CT and high-sensitivity FLI has exhibited unbeatable advantages in cancer theranostics. An integrated microcomputed tomography (microCT) and fluorescence tomography (FT) system for small animal imaging has recently been reported [13]; the bimodal FL and CT imaging are becoming commercially available. Importantly, numerous studies on nanoformulations delivering bimodal (CT and FL) imaging have been performed for disease detection and treatment [12, 14-18]. The nanoplat-forms for drug delivery have opened new avenues in development of a multifunctional and one-piece unified theranostic strategy [1, 3, 13, 14], including the imaging-guided delivery of PSs for PDT [15]. In this regard, the conjunction of a CT imaging contrast agent (CTIA) with a PS might significant potential in anticancer theranostics, as it combines FLI-guided PDT with the 3D imaging capability of CT for localizing the distribution of theranostic agents throughout the body and for visualizing tumor and treatment outputs. However, although numerous nanoformulations for bimodal (CT and FL) imaging have been reported to date, only few studies combine CT/FL imaging and PDT. In particular, Lim and co-authors used the glycol chitosan (GC) conjugated with iodine atom-contained diatrizoic acid (DTA) and PS chlorin e6 (Ce6) to fabricate self-assembled biopolymeric nanoparticles [19]. Although these nanoparticles were shown to have potential for microCT and fluorescence imaging, as well as for PDT, the *in vivo* microCT imaging and PDT were not demonstrated.

One of the most promising drug delivery technologies in oncology research is the development

and utilization of liposomes [11, 20, 21]. Presently various contrast and treatment agents have been encapsulated in liposomes for diagnostics, therapy, and preventive medicine [20]. Specifically, liposomal iodinated CT contrast agents exhibit long residence, very high attenuation, and no significant renal clearance [14, 22]. Meanwhile, the liposomal PS can also lead to more efficient PDT. Compared to the delivery of chemotherapy drugs, which need be released from the nanoparticles for treatment, the encapsulated PS does not need to be released, since the efficiency of PDT depends on the presence of generated ROS that can easily diffuse out of the nanoparticles [23, 24]. In 2000, the liposomal PS (verteporfin) formulation Visudyne® was approved by the U.S. Food and Drug Administration (FDA), and it became the first PDT agent approved for use in the clinical treatment of age-related macular degeneration (AMD) [25]. Recently Hasan's group has introduced a series of liposomal PSs as agents for PDT [20, 26, 27]. In particular, the co-encapsulating approach was utilized to combine verteporfin with a multikinase inhibitor to enhance the photodynamic efficiency through the release of the multikinase inhibitor inside the tumor simultaneously with PDT [28]. Importantly, in a VERTPAC-01 Phase I/II trial, the photochemical activation of Visudyne® within the tumor interstitium was performed under the guidance of CT [29]. The report highlighted that CT imaging can provide very useful information for guiding PDT.

In this study, nanoliposomes (NL) were used as delivery vehicles that co-encapsulated clinically approved iodinated CTIA iodixanol (Visipaque®) and a PS, meso-tetrakis(4-sulphonatophenyl) porphine (TPPS₄), in the interior core to generate the multifunctional nanoformulation for concurrent CT and FL imaging-guided PDT. TPPS₄ has been utilized as it is hydrophilic and can be co-encapsulated with iodixanol within the hydrophilic core of NL. PEGylated lipids are added to the lipid film to form the poly(ethyleneglycol)-modified (PEGylated) NL co-encapsulating iodixanol and TPPS₄ (LIT). The LITs were comprehensively characterized to determine their size, morphology, and photophysical properties as well as their cellular uptake and photo- and dark-cytotoxicity. results showed that the co-encapsulation of PS and iodinated CTIA within LIT can cause enhanced singlet oxygen generation due to the intraparticle heavy atom (iodine) effect on the PS, which results in enhanced PDT efficacy of cancer cells *in vitro*. The biodistribution of LIT and tumor targeting ability in mice was assessed by *in vivo* CT/FL bimodal imaging. Owing to the PEGylation and other structure-related peculiarities, the prepared

LITs were found to have an enhanced passive tumor uptake by the enhanced permeability and retention (EPR) effect [30], along with insignificant accumulation in the liver and other organs. The highly tumor-specific biodistribution of LIT was manifested by both FL and CT imaging, demonstrating the applicability of LITs as contrast agents for bimodal tumor imaging, along with a possibility of imaging-guided systemic delivery of therapeutics (e.g., PS) to the tumor. Importantly, PDT, which was performed with tumor-bearing mice intravenously (i.v.) injected with different TPPS₄ formulations, revealed high efficacy of LIT. Our study demonstrates that LIT is a highly promising theranostic nanoformulation that allows for tumor-specific delivery and retainment of PS and CTIA for enhanced FL and CT bimodal imaging-guided PDT of cancer.

Results and Discussion

Synthesis and characterization of LIT

LIT were fabricated by encapsulating a CT contrast agent (iodixanol) and a PS (TPPS₄) in the sterically stabilized moderately cationic PEGylated liposomes (Figure 1A) produced with 1,2-dipalmitoyl-sn-glycero-3-phosphocholine (DPPC), 1,2-dioleoyl-3-trimethylammonium-propane (chloride salt) (DOTAP), 1,2-distearoyl-sn-glycero-3-phosphoethanolamine-N-[amino(polyethylene, glycol)-2000] (ammonium salt) (DSPE-PEG2000) and cholesterol, as described in the Methods. In the liposomes, cholesterol was added to the NL formulation to modulate membrane permeability and biological stability [31]. Meanwhile, DSPE-PEG2000 was doped in the lipid film to form the PEGylated liposomes. PEGylation can alter biodistribution, prolong circulation half-life, and avoid recognition and subsequent capture of the liposomes by the reticuloendothelial system (RES) [32]. In addition, NL with the same phospholipid composition containing only TPPS₄ (LT) were prepared for the control experiments.

The prepared NL were further characterized by dynamic light scattering (DLS). The obtained characteristics (size, zeta-potential and, percentage of the loaded iodixanol and TPPS₄) are listed in Table 1. The averaged diameter of LT and LIT was found to be 111.0 nm and 117.1 nm, respectively. The close sizes of LT and LIT demonstrate that the co-encapsulation of iodixanol with TPPS₄ in the interior aqueous core does not significantly affect liposome formation. This can also be evidenced by the NL size distribution: the diameter of the fabricated NL varies between 50 and 200 nm, with most of them in 90-120 nm range (Figure S1). This size is considered as appropriate for enhanced permeation through the leaky tumor

vasculature [33]. The NL in our study are slightly cationic with a zeta potential above 10 mV (Table. 1) due to the DOTAP in the lipid composition [34], which can enhance the NL stability and efficiency of drug delivery [35]. The transmission electron microscope (TEM) images (Figure 1B) illustrate the structure of NL with the size close to 150 nm, which is in the range determined by DLS. It can also be noted that the presence of the heavy atom (iodine)-rich CTIA within LIT results in higher TEM contrast for the interior core, as compared to LT nanoliposome without iodine (Figure 1B).

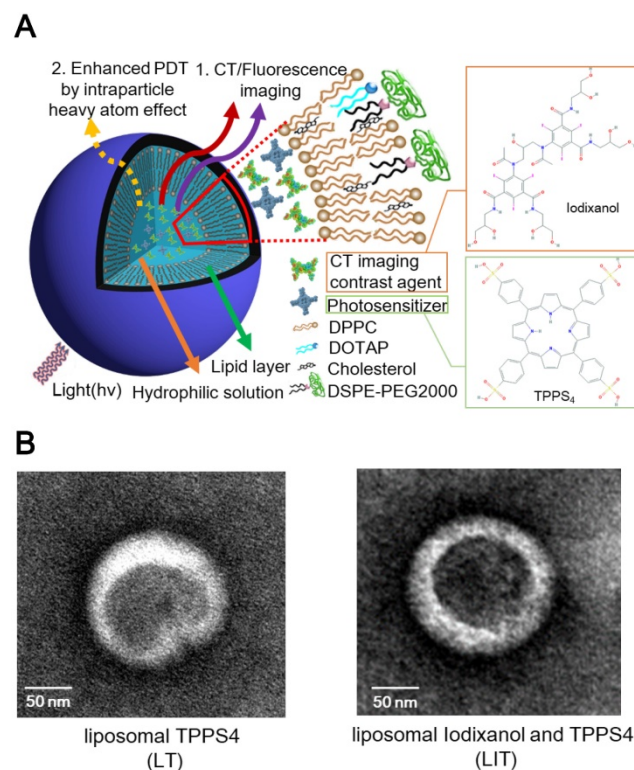


Figure 1. (A) The schematic diagram illustrating nanoliposomes co-encapsulating the CTIA and PS. (B) Transmission electron microscopy (TEM) images of TPPS₄ in NL (LT) and NL co-encapsulating iodixanol and TPPS₄ (LIT).

Table 1. Nanoliposome size, zeta-potential, loading percentage of TPPS₄ and iodixanol.

NL	Size (nm)	Zeta potential (mV)	TPPS ₄ loading (%)	Iodixanol loading (%)
LT	111.0±0.6	16.0±0.1	72.7±1.5	0
LIT	117.1±0.7	13.5±0.4	67.1±6.2	63.5±3.8

NL - nanoliposomes; LT - nanoliposomes encapsulating TPPS₄; LIT - nanoliposomes co-encapsulating iodixanol and TPPS₄.

The absorption spectra of free TPPS₄ (T), LT and LIT in PBS (pH=7.4) are presented in Figure 2A. All types of NL show a strong absorption maximum at 420 nm and two peaks at around 552 nm and 640 nm, which are characteristic for TPPS₄. Correspondingly, TPPS₄ in NL manifests fluorescence peaks at ~660 nm. It is worth noting that the TPPS₄ emission from LT

and LIT is almost identical although it is slightly different from the free TPPS₄ fluorescence (Figure 2B).

The concentration of TPPS₄ in LT and LIT was estimated using the known absorptivity (molar extinction coefficient, MEC) of TPPS₄ in DMSO solution (Figure S2A). Liposomal formulations were dissolved in DMSO to break NL and release TPPS₄, and then its absorption spectra were acquired and compared with those of free TPPS₄ in DMSO.

The TPPS₄ loading efficiency in NL was determined as a percentage of the PS encapsulated in the NL to the whole PS amount used for NL preparation. The results are listed in Table 1. The TPPS₄ loading efficiencies in LT and LIT were determined to be 72.7±1.5% and 67.1±6.2%, respectively. The similar loading efficiencies for LT and LIT suggest that the presence of CTIA does not significantly affect the encapsulation of TPPS₄ in the hydrophilic core during the extrusion process. We also compared the leakage of the PS from NL at different storage conditions and found that the leakage was slow. At 4°C storage, the leakage of TPPS₄ from LT and LIT is less than 5.0% after a one week storage period and less than 10.0% from both NL formulations after an extended storage period of 40 days (Figure S3A). Meanwhile, at more physiological conditions [37 °C with 10% fetal bovine serum (FBS)], the leakage of TPPS₄ from LT and LIT increases and reaches ~45% (from the initial amount) after ~48 hours, and then it significantly slows down and remains up to 50% even after 240 hours (Figure S3B).

To calculate the concentration of iodixanol in LIT, the CT phantom images of iodixanol were acquired using its PBS dispersions at various concentrations. The CT intensity at the imaging area increases linearly with the increase in iodixanol concentration (Figure S2B). Using the linear dependence of CT values on the iodixanol concentration, we obtained the X-ray absorption/concentration dependence for free iodixanol. The CT values for iodixanol in NL were also measured, and the concentrations of iodixanol in NL were determined using the linear dependence for free iodixanol as a calibration curve. The iodixanol loading efficiency in liposomes was calculated as a ratio percentage between the concentration of iodixanol in the NL and the initial concentration of iodixanol used for the NL preparation. The iodixanol loading efficiency in LIT is about 63.5±3.8% (Table 1). We also examine the leakage of CT contrast agents from the NL. At the storage conditions (4 °C), the leakage of iodixanol from LIT is around 3-4% for a one week storage period and increase to 8-9% with an extended storage period of 40 days post fabrication (Figure S3C). At physiological

conditions, the leakage of iodixanol from LIT is up to ~45% at 96 hours and then strongly slows down, up to 50% after 240 hours (Figure S3D).

It should be noted that although the significant leakage from the NL is observed only at later time points, no significant changes in the size and zeta potential of NL (LT or LIT) are observed during 40 days at 4 °C (Figures S4A and B), indicating the excellent storage stability of NL. The polydispersity index (PDI) of LT or LIT is lower than 0.1 and does not noticeably change during storage, indicating the absence of aggregation (Figure S4C). For all the studies described henceforth, the NL are freshly prepared, characterized, and used within five days from preparation to ensure stability and consistency of the experiments.

Evaluation of singlet oxygen generation by LIT

The ability of the PS to generate reactive oxygen species is a key factor in PDT [36]. Singlet oxygen is a main cytotoxic agent in PDT and the correlation between singlet oxygen generation during PDT and the post-PDT biological response has been demonstrated and reviewed extensively [37,38]. Singlet oxygen is produced through the interaction between the long-lived triplet state of PS and molecular oxygen in the surroundings. Since the triplet electronic PS molecule is in an excited state as a result of intersystem crossing (ISC) from the photoexcited singlet electronic state of PS, the quantity of the generated singlet oxygen is dependent on the ISC efficiency [39]. The rate of ISC can be increased by enhancing the spin-orbit coupling when heavy atoms (e.g., iodine) are close enough to the pi-electron system of the PS (intraparticle heavy atom effect) [19, 39].

To examine the influence of iodinated CTIA on the PDT efficiency of TPPS₄, the singlet oxygen generation by TPPS₄ was first assessed using the water soluble anthracene derivative, 9, 10-anthracenediyl-bis(methylene)dimalonic acid (ABDA). When ABDA and singlet oxygen interact, the anthracene moiety undergoes a specific reaction to form a 9, 10-endoperoxide product. This singlet oxygen-specific reaction can be assessed spectrophotometrically by measuring the decrease in optical absorbance at 380 nm (the absorption peak of anthracene chromophore) [24, 40, 41]. The use of ABDA to detect and quantify singlet oxygen production through the decrease in the absorption at 380 nm has been reported [42]. As seen in Figures 3A, S5 and S6A, the ABDA absorption at 380 nm for different TPPS₄ formulations decreases faster under 552 nm laser irradiation than under the 640 nm one, for the same laser power density of 50 mW cm⁻². Since TPPS₄ absorbs light stronger at 552

nm than at 640 nm (Figure 2A), these data confirm that the singlet oxygen production correlates with the absorption of TPPS₄. Meanwhile, on assessing singlet oxygen-specific ABDA bleaching in different NL formulations that contain the same amount of TPPS₄ under the same irradiation, we found that ABDA in an LIT water dispersion bleaches faster than in an LT dispersion (both for 552 nm and 640 nm laser irradiation), suggesting that LIT produces more singlet oxygen than LT.

To avoid the potential influence of ABDA on the singlet oxygen production by TPPS₄, the singlet oxygen generation potential of TPPS₄ was also directly evaluated by the singlet oxygen phosphorescence emission at 1270 nm [40, 43, 44]. Figure 3B shows time-resolved signals from the singlet oxygen phosphorescence produced by LT and LIT nanoformulations under laser excitation at 532 nm. As can be seen, LIT produces a significantly higher phosphorescence signal, which corresponds to the higher amount of singlet oxygen sensitized by TPPS₄ within LIT. Although the comparison of singlet oxygen generation by LT and LIT has ruled out the possibility that the singlet oxygen production by TPPS₄ is affected by liposomal bilayer rather than the presence of iodixanol, we have additionally inspected the effect of iodixanol on singlet oxygen generation by TPPS₄ in solution (without liposomes). As shown in Figure S6 in Supplementary materials, the presence of the iodixanol in the TPPS₄ solution does result in enhanced singlet oxygen production. Consequently, taken together, the results of singlet oxygen measurements reveal that the presence of iodinated CTIA in NL can increase the singlet oxygen generation by the NL encapsulated TPPS₄. Similar enhanced singlet oxygen generation has been demonstrated for other nanoformulations co-encapsulating iodinated molecules and PS. This enhancement is due to increased ISC rate in the PS molecule produced by the

spin-orbit coupling enhanced by external iodine atoms (heavy atom effect) [19, 39, 45].

Internalization of LIT by cancer cells *in vitro*

The uptake of T, LT, and LIT by cancer cells *in vitro* was assessed using confocal microscopy and measurements of TPPS₄ fluorescence signals from cells. Figure 4A shows merged confocal transmission/fluorescence images of HeLa cells treated after 18 hours of incubation with T, IT, LT and LIT, where the fluorescence signal from TPPS₄ is marked in red pseudocolor. The figure confirms that PS molecules in both free and liposomal formulations are internalized by cancer cells after 18 h incubation, similarly to the previously reported results [46]. Strauss *et al* have examined the intracellular fluorescence behavior of TPPS₄ and discovered that it is mainly localized in the cell lysosomes [47]. Our imaging results show a comparable pattern of the intracellular localization for both free and liposomal TPPS₄, suggesting that TPPS₄ delivered with LT and LIT is localized inside cells in a similar way. However, it should be noted that the TPPS₄ fluorescence signal from cells is more intense for liposomal nanoformulation (LT and LIT), suggesting that encapsulation in NL is favorable for internalization of TPPS₄ by cancer cells *in vitro*. To validate this, we evaluated the uptakes of all TPPS₄ formulations by measurements of the TPPS₄ fluorescence from the collected and lysed cells. As shown in Figure S7, the fluorescence signal from the cells (which correlates with cellular uptake of TPPS₄) increases during ~18 hours of incubation of cells with TPPS₄ formulations. The intracellular fluorescence intensity of LT and LIT samples is very close to each other, indicating that uptake of TPPS₄ is also very similar for these NL. Meanwhile, it is also significantly higher than the FL signal from free TPPS₄ samples, indicating that TPPS₄ in NL is internalized by the cells more efficiently than the free drug.

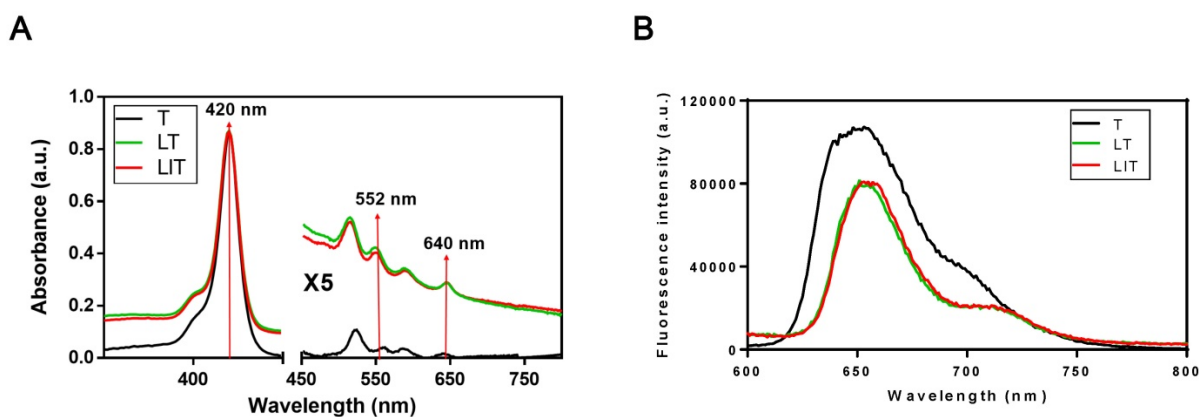


Figure 2. (A) Absorption spectra of free TPPS₄ (T), TPPS₄ in NL (LT), and NL co-encapsulating iodixanol and TPPS₄ (LIT) in PBS. (B) Fluorescence spectra of T, LT, and LIT in PBS. Ex=420 nm.

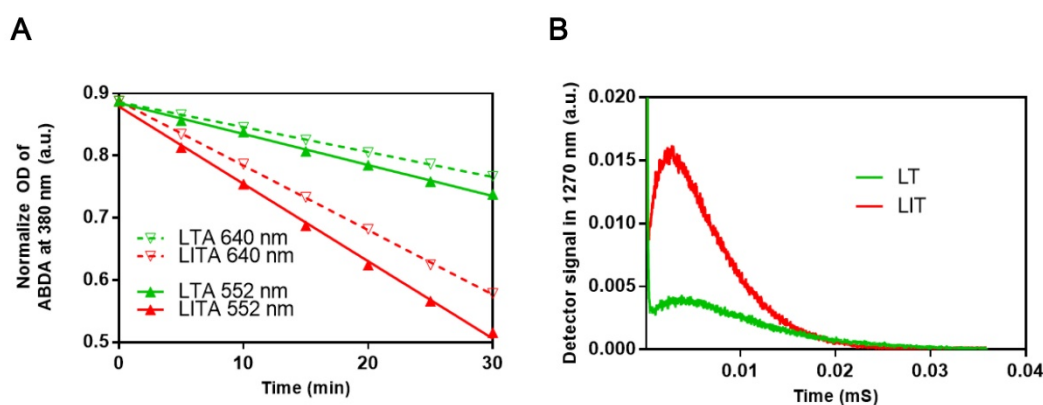


Figure 3. (A) Comparison of ABDA bleaching as a measure of the singlet oxygen generation in LT dispersion (LTA) and LIT dispersion (LITA). (B) Decays of singlet oxygen phosphorescence at 1270 nm illustrating the singlet oxygen generation by LT and LIT.

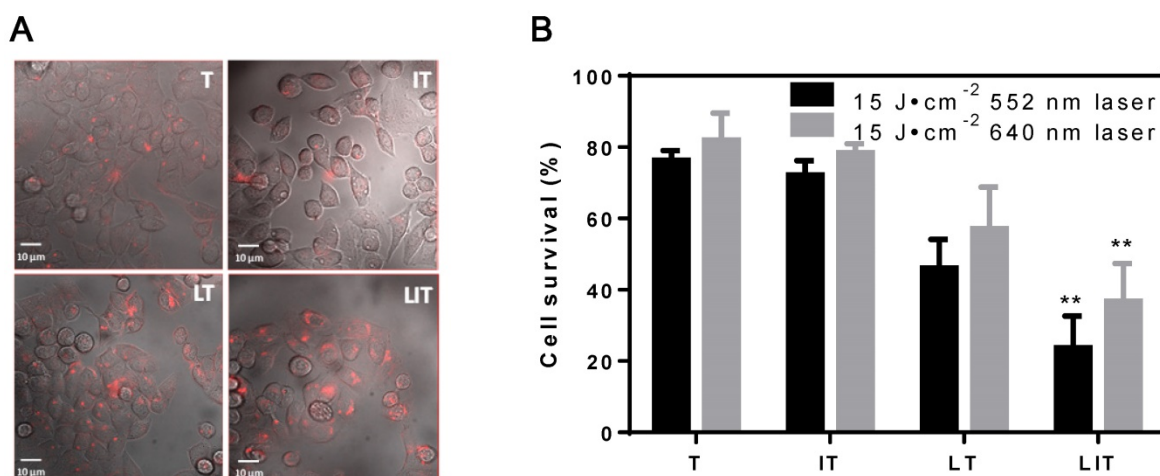


Figure 4. *In vitro* cellular uptake and PDT of HeLa cells treated with free TPPS₄ (T), free iodixanol and TPPS₄ (IT), TPPS₄ in NL (LT), and NL co-encapsulating iodixanol and TPPS₄ (LIT). (A) Cellular internalization of TPPS₄ after 18 h incubation with T, IT, LT, or LIT. Images merging the transmission and fluorescence confocal channels are shown. Fluorescence of TPPS₄ (red pseudocolor) was excited by a 543 nm laser. (B) HeLa cells survival one day post-PDT. The dark bars indicate 552 nm laser irradiation and the light ones indicate 640 nm laser irradiation at the same irradiation dose (15 J cm⁻²). (**p < 0.01 compared with T, IT and LT at the same laser irradiation dose).

Evaluation of photo-toxicity and drugs toxicity

The cell viabilities were assessed with Cell Counting Kit-8 (CCK-8) 24 h after treatment with liposomal or free TPPS₄. No cell death was observed under laser irradiation (15 J cm⁻²) at 552 nm or 640 nm (Figure S8A) for the control (untreated) groups. No significant dark toxicity was found for HeLa cells or 4T1 cells incubated with a high concentration (40 μM) of free or liposomal TPPS₄ (Figure S8B).

The efficiency of PDT *in vitro* was also inspected; Figure 4B shows the post-PDT cell survival results under laser irradiation at 552 nm and 640 nm. First, the cell survival percentage in the free TPPS₄ group was ~76% and 82% under laser irradiation at 552 nm and 640 nm, respectively. Second, PDT with combination of free TPPS₄ and iodixanol resulted in 72% and 78% cell survival under laser irradiation at 552 nm and 640 nm. Such a small difference between

the phototoxicity of free TPPS₄ and TPPS₄/iodixanol combination can be expected. Since the heavy atom effect arises from the interaction between pi-electron system of TPPS₄ and iodixanol molecules (which can occur when molecules are in close proximity), it is unlikely that such proximity can be achieved inside cells for tolerable concentrations of free iodixanol and TPPS₄, without initial co-localization within liposomes. Next, the LT group showed ~46% and ~57% cell survival percentage under 552 nm and 640 nm, respectively, indicating that the liposomal TPPS₄ have higher PDT efficiency. This correlates with the higher cellular uptake of the liposomal TPPS₄, which was shown by confocal microscopy and cellular uptake measurements. Finally, the cell survival percentage of the LIT group under laser irradiation at 552 nm and 640 nm was measured to be ~23% and ~37%, respectively. This means that LIT nanoformulations have a significantly higher ability to eradicate cancer

cells compared with LT and T under the same irradiation. This increase in PDT efficiency cannot be caused by the increase in cellular uptake, as it is shown to be similar for LT and LIT. Thus, one can conclude that the NL-co-encapsulated iodinated CTIA significantly enhances the PDT efficiency of the TPPS₄ delivered to cells within the NL, which correlates with the enhanced generation of singlet oxygen.

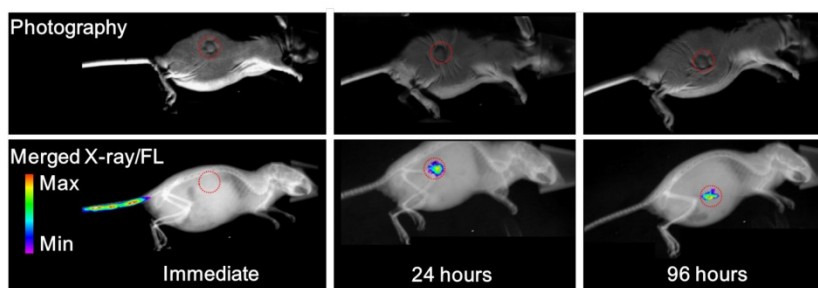
In vivo and ex vivo fluorescence imaging of LIT

To compare the *in vivo* FL imaging capability and tumor targeting ability of different formulations, free T, LT and LIT were respectively i.v. injected in BALB/c tumor-bearing mice. The results of the *in vivo* FL imaging are shown in Figures 5A and S9. The fluorescence images of the mice were taken at different time points post injection and merged with the corresponding high-resolution X-ray images taken at the same time point to serve as a background image. The fluorescence images manifestly demonstrate the feasibility to detect and image the spectrally distinguished fluorescence of TPPS₄ (shown in red circle) in the LIT (Figure 5A) and LT (Figure S9B) injected groups. Figures 5A and S9B illustrate that enhanced FL signals from the liposomal formulations are detected in the tumor site at 24 and 96 hours post injection, whereas the images captured

immediately after injection showed that the distinct fluorescence signal can be detected at the injection site (tail). In contrast, for the control (free TPPS₄) group, no FL signal can be identified at 24 and 96 hours post injection, although it was visible at the tail injection site immediately after injection (Figure S9A). The FLI results indicated that liposomal TPPS₄ can accumulate in the tumor over a longer time period (24-96 h post-injection), which can be attributed to the prolonged circulation time of the PEGylated liposomes [20,48], and the related improvement of the passive tumor targeting due to the EPR effect [49].

Ninety six hours post injection of LIT and acquisition of the corresponding CT and FL imaging, the organs were resected and imaged immediately. The results of the *ex vivo* fluorescence imaging are shown in Figure 5B. The imaging results from the major organs validate that the LIT accumulates mainly in the tumor. The amount of FL signals observed in the kidney, liver, and spleen were significantly lower than that from the tumor, demonstrating a high efficiency of the passive tumor targeting with LIT. The relative amount of FL signal from the lungs and the heart was even lower. It should be noted that the liposomal formulation of TPPS₄ has been reported to have higher efficiency in *in vivo* PDT in comparison with free TPPS₄, and the results were attributed to the liposome-mediated delivery, which increases the PDT efficacy [50].

A



B

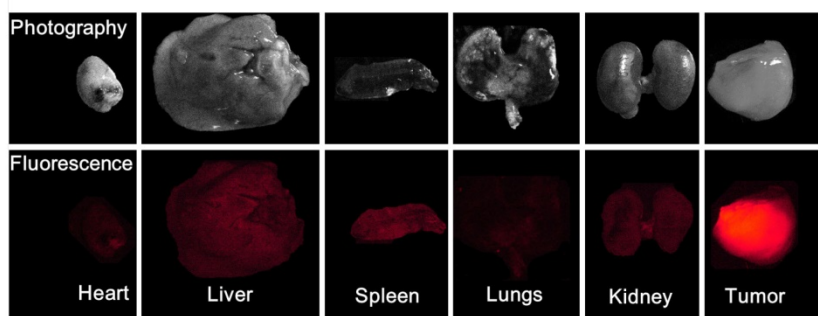


Figure 5. (A) Photography and X-ray/fluorescence (X-ray/FL) images of a nude mouse with a tumor at various time points (2, 24, and 96 h) post injection with NL co-encapsulating iodixanol and TPPS₄ (LIT). Red circles indicate the tumor tissue. (B) Photography and fluorescence images of the major organs resected from mouse 96 h post-injection.

In vivo micro-CT imaging of LIT

The accumulation of free iodixanol and LIT in both normal tissue and in mouse tumors were non-invasively investigated by CT imaging (Figure 6). The kidneys can be observed very quickly after the immediate imaging and the bladder is also visible 30 min after the mice are injected with the free iodixanol, illustrating its fast renal clearance. It is shown to be rapidly eliminated from the kidneys and bladder at 60 min, and no CT signal from iodixanol was detected after 24 h, suggesting that this kind of free CTIA is not suitable for time-lapse monitoring of specific organs and diseased sites.

Although the accumulation of iodixanol was not seen immediately after LIT injection, the tumor strikingly appeared in the CT image taken 30 min post-injection, indicating a burst in the uptake. The kidneys and

bladder were visible at the 60 min point, suggesting that some iodixanol may have been released from the NL. However, no significant signal could be detected from the kidneys and bladder 24 h after injection. At the same time, the tumor tissue was brightly highlighted even after 96 h, demonstrating the major accumulation and retention of LIT in the malignant tissue. Such high tumor targeting efficiency and specificity of LIT distribution can be associated with the enhanced permeability in tumor vasculature along with slow clearance, which provides an adequate environment for accumulation and retention in the tumor bed [12]. It is worth noting that the iodine-containing, DTA-conjugated GC nanoparticles (similar to those reported by Kim's group [19]) were recently examined by Choi and co-authors as a novel type of nanoparticles for the CT/ultrasound bimodal imaging of tumor [51]. Meanwhile, the enhancement of CT contrast was found to be not significant. This is apparently associated with the limited amount of iodine-contained DTA moieties that can be conjugated within GC nanoparticles. In this context, our nanoplatform, which can be loaded with iodixanol molecules at high concentration, has the clear advantage.

In vivo phototherapy effect evaluation

To evaluate the PDT efficacy of LIT *in vivo*, the same amount of free or liposomal TPPS₄ was i.v. injected in tumored mice, which were then exposed to 640 nm laser irradiation. The tumor growth results after treatment are shown in Figure 7A. In a remarkable contrast with other groups, a significant suppression of tumor growth was exhibited for the group of mice injected with LIT and then irradiated. The photographs of tumor-bearing mice receiving various treatments persuasively illustrate the striking difference between the tumors treated with PDT with LIT and other TPPS₄ formulations (Figure S10). The enhanced PDT efficacy with LIT as PS indicates that the developed nanoliposomal formulation has highly promising potential for cancer treatment. The weight of mice showed no significant difference between various groups (Figure 7B), indicating that the treatment with TPPS₄ formulations were well tolerated by the animals. In addition, to assess the *in vivo* toxicity, major organs (liver, lung, spleen, kidney, and heart) were excised from LIT-treated and control (PBS injected) mice at 7 days after i.v. injection and histopathological changes in the major organs were evaluated by hematoxylin and eosin (H&E) staining. No pathological changes in H&E images were detected in the LIT treated group as compared to that from the control group (Figure S11), demonstrating that LIT formulation was safe at the utilized dose.

It should be noted that the similar intraparticle heavy-atom (iodine) effect on PS have been investigated by several groups. An encapsulation of the hydrophobic photosensitizer in iodine-concentrated nanoparticles (organically modified silica) to enhance the PDT efficacy through the intraparticle heavy-atom effect has been first reported by Prasad's group [39]. Following this, Kim's group developed DTA-conjugated GC nanoparticles and iodinated pluronic (F-127) nanoparticles encapsulating PS (Chlorine e6) to enhance PDT efficacy [19, 45]. Iodinated silica/porphyrin hybrid nanoparticles were later described, which inhibited tumor growth *in vivo* under LED irradiation as a result of the iodine-enhanced PDT combined with photothermal therapy [52]. However, the CT imaging capability of reported iodinated nanoplatforms for PDT is very limited and no CT imaging guided PDT based on these nanoplatforms has been performed. It should also be noted that the clinical perspectives of all these reported nanoformulations are far from being visible, since their biocompatibility and biodegradability need be inspected in a time and cost consuming way. In contrast, our research utilizes the clinically approved CT imaging agent along with clinically acceptable liposomes and therapy agent (which can also be replaced with other water-soluble PS) to accomplish imaging guided cancer therapy. Furthermore, the molar ratio of different reagents for our nanoplatform can be feasibly adjusted to achieve enhanced biomedical imaging and highly efficient PDT. The flexible, biocompatible and biodegradable nanoplatform based on clinically approved agents brings a strong promise for clinical cancer theranostics.

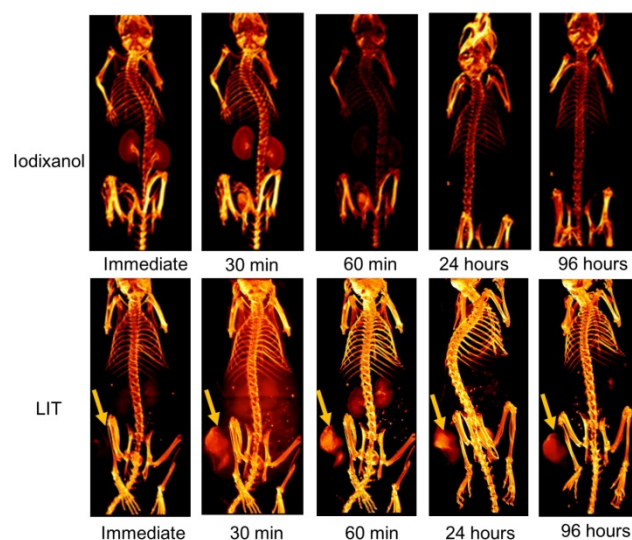


Figure 6. Three dimensional volume-rendered images of the nude mice bearing HeLa tumor xenografts and injected with free iodixanol or NL-co-encapsulated iodixanol and TPPS₄ (LIT) into the tail vein. Arrows indicate the location of the tumor.

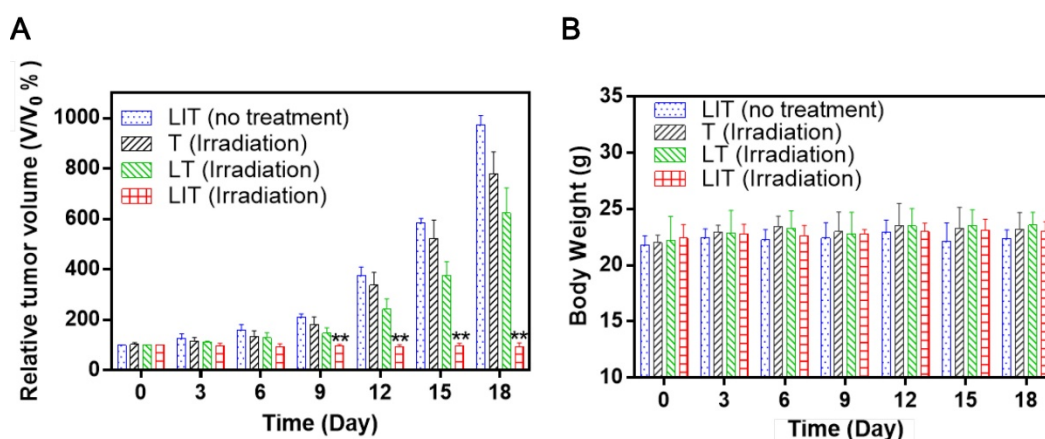


Figure 7. *In vivo* PDT using T, LT, and LIT on HeLa tumor xenografts. (A) The growth of xenograft tumors in different groups (n = 5). (**p < 0.01 compared with other groups on the same day). (B) Body weight change in mice under different treatments 18 days after injection.

Conclusions

The development in nanotechnology and multimodal biomedical imaging research have enabled us to introduce a new theranostic approach to enhance PDT of cancer, guided by CT and FL bimodal imaging. The NL co-encapsulating iodinated CTIA and PS have been designed with the goal to enhance PDT efficacy by the heavy atom effect of iodine, and to provide nanoformulations with CT and fluorescence imaging contrasts. The designed NL (LIT) are cationic PEGylated NL that have shown a significantly higher singlet oxygen yield and photodynamic efficiency (both *in vitro* and *in vivo*) than the PS in nanoliposomal formulation without CTIA. Furthermore, the fluorescence and X-ray absorption properties of LIT make it an efficient contrast agent for optical and CT tumor imaging and imaging-guided cancer PDT in small animals (mice). Since the clinically approved iodinated CTIA has been co-encapsulated with the commercially available PS within liposomes, which are the most popular clinically accepted class of nanosized drug delivery vehicles [20], LIT has a high potential for clinical translatability as a multifunctional theranostic agent. Our future work will involve evaluation of LIT based preclinical therapy to develop enhanced, multimodal imaging-guided PDT for cancer.

Materials and Methods

Materials

DPPC, DSPE-PEG2000, DOTAP, cholesterol and polycarbonate membranes (100 nm pore size) were purchased from Avanti Polar Lipids Inc (Alabaster, AL). VISIPAQUE® (iodixanol injection) was obtained from GE Healthcare Ireland (Cork, Ireland). TPPS₄ was purchased from Frontier Scientific (Logan, UT). ABDA, chloroform and dimethyl sulfoxide (DMSO)

were purchased from Sigma Aldrich (Saint Louis, MO). Float-A-Lyzer G2 dialysis device was obtained from Spectrum® Laboratories (Rancho Dominguez, CA). Phosphate-buffered saline (PBS, pH 7.4), fetal bovine serum (FBS), Dulbecco's Modified Eagle Medium (DMEM), Roswell Park Memorial Institute 1640 (RPMI 1640), trypsin-EDTA and penicillin-streptomycin were purchased from Gibco Life Technologies (AG, Switzerland). Solvable solubilizer was purchased from PerkinElmer (Waltham, MA). Cell Counting Kit-8 (CCK-8) was obtained from Dojindo (Kumamoto, Japan).

Synthesis of NL

DPPC, DSPE-PEG2000, DOTAP, and cholesterol at a molar ratio of 10:1:1:5 were mixed in chloroform and then the chloroform was evaporated by using a rotary evaporation system to make a thin lipid film. This film was hydrated with a solution containing 0.7 mL of 0.4 M iodixanol and 0.3 mL of 1.0 mM TPPS₄ in PBS. The hydrated solution was then subjected to freeze-thaw cycles (4-45 °C) to encapsulate TPPS₄ and iodixanol. The dispersions were extruded through polycarbonate membranes at 42 °C to form unilamellar vesicles. Non-encapsulated agents were separated from the LIT by using the Float-A-Lyzer G2 dialysis device at 4 °C. Liposomes containing TPPS₄ alone (LT) were also prepared separately using the method described above.

Characterization of NL

The absorption and fluorescence spectra were acquired using a spectrophotometer (LAMBDA 750 UV/VIS/NIR, PerkinElmer) and spectrofluorometer (Fluorolog-3, Horiba), respectively. The molar extinction coefficient (MEC) of TPPS₄ at 420 nm was determined according to the absorption and concentration standard curve of TPPS₄. The concentration of TPPS₄ in NL was calculated according to its MEC.

Drug release at the storage or physiological conditions was monitored through dialysis in PBS at 4 °C or in PBS with 10% fetal bovine serum at 37 °C, respectively. The TPPS₄ leaking out of the stored NL was measured by dialyzing free TPPS₄ in the dialysis device at different time intervals. The residual concentration of PS inside the NL was determined by measuring its absorption spectrum after dialysis. The leakage of PS from the NL was estimated by subtracting the residual concentration from the original concentration. The CT image in the phantom study was acquired using micro CT (SuperArgus, Sedecal) with these imaging parameters: 300 μ A of current, 50 KV of voltage, 33 μ m of resolution, and 300 ms of exposure time. The residual concentration of iodixanol inside the NL was determined by measuring their CT intensity after the dialysis. The leakage of iodixanol from the NL was determined by subtracting the residual concentration from the original concentration.

The size, polydispersity index (PDI), and zeta potential of NL were estimated by the dynamic light scattering (DLS) using a particle size analyzer (Zetasizer Nano ZS, Malvern). The morphologies of liposomes were assessed using transmission electron microscopy (TEM). For NL to be imaged with TEM, 10 μ L of NL solution was dropped onto the carbon support films stabilized with formvar and negatively stained using 2 μ L 1% uranyl acetate. The carbon support films were air-dried and washed with 5 μ L of pure water. The images were obtained by operating at an acceleration voltage of 100 kV on TEM (JEM-1230, JEOL).

Singlet oxygen measurements

Chemical oxidation of ABDA was utilized to characterize the singlet oxygen generation efficiency of free and liposomal PSs. ABDA is known to form the corresponding endoperoxide by singlet oxygen bleaching [53]. In this study, sample solutions with the same TPPS₄ concentration (7.5 μ M) were mixed with 0.06 mM ABDA in PBS. An absorbance decrease of ABDA at 380 nm was measured as a function of time on the LAMBDA 750 UV/Vis/NIR Spectrophotometer, under irradiation with a 552 nm or 640 nm diode laser (OBIS, Coherent). During experiments, all samples were added into quartz cuvettes with a 1 cm path length.

Singlet oxygen generation was also evaluated directly via its phosphorescence emission that peaked at 1270 nm [40, 44]. A Fluorolog-3 spectrofluorimeter attached with a spectrometer (iHR320, Horiba) for infrared range was employed to detect singlet oxygen emission. A singlet oxygen phosphorescence was detected by the thermoelectrically cooled NIR-PMT

detector (H10330B-75, Hamamatsu) of the iHR320 spectrometer that was set to 1270 nm and singlet oxygen phosphorescence decays under pulsed laser excitation were directly recorded by the Digital Phosphor Oscilloscope (TDS 3034C, Tektronix) coupled to the output of the NIR PMT. The same TPPS₄ concentration (0.2 mM) of sample suspensions were placed in a quartz cuvettes, which were excited by the nanosecond Nd:YAG pulsed laser at 532 nm (LS-2137, Lotis TII) with a 10 Hz repetition rate. The emission signal was detected at 90° relative to the excitation laser beam. Additional long pass (LP) filters (950 LP and 538 AELP, both from Omega Optical) were employed to attenuate the scattered light and fluorescence from the samples.

Cell culture and *in vitro* uptake of drugs

HeLa and 4T1 cell lines were incubated in complete Dulbecco's Modified Eagle Medium (DMEM) and RPMI1640 (containing 10% (v/v) fetal bovine serum and 1% (v/v) 5000 I.U. per mL penicillin/streptomycin) at 37 °C in a 5% CO₂ incubator.

To compare the cellular uptake of TPPS₄ in different formulations, 1 mL of DMEM containing 10 μ M of free or liposomal TPPS₄ was added to the cells in the 35 mm cell culture dishes under low-light conditions (to avoid photosensitization of the cells or photobleaching of the PS). The cells were incubated with PS-contained media for time intervals ranging from 0 to 24 h. Every group was tested in four-fold replicates. At every time point, the medium was removed and cell dishes were rinsed with PBS three times. The 0.5 mL of aqueous-based tissue solubilizer (Solvable from PerkinElmer) was then added to dishes to lyse the cells. After the cells were completely lysed, the solutions were removed from the dishes and their fluorescence spectra in the 600-800 nm range were measured by a Fluorolog-3 spectrofluorimeter, using excitation light at the wavelength of 420 nm. After obtaining spectra, the areas under fluorescence curves were integrated for every sample to evaluate the amount of TPPS₄ taken by the cells. All experiments were repeated at least three times.

For visualization of PS cellular uptake with confocal microscopy, HeLa cells were cultured in 35 mm cell culture dishes with glass bottoms (NEST, Jiangsu, China) over night at ~50% confluency, 1 mL complete DMEM containing 10 μ M of the different formulations of TPPS₄ (i.e., free TPPS₄, free TPPS₄ and iodixanol, LT or LIT) was added to the cell culture dishes and incubated for 18 h. Post incubation, cells were rinsed three times by washing in PBS and then DMEM was added. Immediately after this, the confocal fluorescence images were obtained by using a laser scanning confocal microscope (TCS SP2, Leica).

In vitro cytotoxicity assay

Cytotoxicity of different PS formulations were assessed using the commercial CCK-8 cell viability test. CCK-8 kits contain a water-soluble tetrazolium salt (WST-8) that can be reduced to a yellow colored formazan dye by dehydrogenase activity [54]. Firstly, HeLa and 4T1 cells were diluted to a cell density of 10^5 cells/mL and seeded in 96 well cell culture plates (100 μ L per well). The cells were maintained at 37 °C in a 5% CO₂ cell incubator for 24 h. Then, the old media was discarded and 100 μ L of fresh culture medium containing 10 μ M free or liposomal TPPS₄ was added and the cells were incubated in the dark for 18 h. After incubation, the cells were rinsed with PBS. Thereafter, 100 μ L of fresh culture medium was added to every well of the 96 wells cell culture plates. For the laser irradiation groups, cells were irradiated with a custom laser irradiation system. Light was delivered by 552 nm or 640 nm fiber-coupled diode lasers (OBIS, Coherent) with 50 mW·cm⁻² laser power density. All the cell plates were then maintained for 24 h at 37 °C in a 5% CO₂ cell incubator. The next day, all the wells in the cell culture plates were refed with 100 μ L completed cell culture medium containing 10 μ L CCK-8 solution. Cell survival was estimated by the absorption of every well at 450 nm using a multimode microplate reader (Spark®, Tecan). Four replicates for each group were run. The same cytotoxicity experiment was repeated separately three times. Dark toxicity of the PS and control groups were assessed in the same manner, excluding laser irradiation.

In vivo tumor implantation

All animal experiments were approved by the Institutional Research Animal Care and Use Committee of the University of Macau. The female BALB/c nude mice (Source: The Jackson Laboratory, USA) were bred under dark and aseptic conditions in a small animal facility. Tumor implantations was prepared by subcutaneously injecting 50 μ L PBS (containing 10^7 HeLa cells) above the hind leg.

Histological analysis

For the assessment of *in vivo* toxicity, major organs (heart, liver, spleen, lungs, and kidneys) were excised from the mice injected with LIT or PBS (control group) at 7 days post injection, fixed in 4% formalin, and then embedded in paraffin. Subsequently, the sliced organs were stained by Hematoxylin and Eosin (H&E) and imaged under a light microscope (Ts2, Nikon).

In vivo and ex vivo fluorescence imaging

Before fluorescence imaging, 0.2 mL of the different reagents (all contained 0.16 mg·kg⁻¹ TPPS₄)

were injected through the tail vein. All mice were anesthetized by isoflurane. The biodistribution of different reagents were investigated by fluorescence imaging at different time points after drug injection. The mice were sacrificed after 96 h. Major organs and tumors were immediately extracted and imaged. The distribution of TPPS₄ in major organs and in the tumors was assessed *ex vivo*. *In vivo* and *ex vivo* fluorescence images were acquired using a preclinical optical/X-ray imaging system (*In vivo* Xtreme, Bruker) by using 420 nm as the excitation filter (band-pass \pm 10 nm) and 700 nm as the emission filter (band-pass \pm 17.5 nm).

In vivo CT imaging

Two hundred microliters of free iodixanol at the same iodine concentration (1.1 g·Kg⁻¹) or LIT was injected through the tail vein. All the imaging groups were anesthetized by isoflurane and imaged by a preclinical CT System (SuperArgus, Sedecal). Imaging parameters were as follows: 50 KV, 300 μ A, 33 μ m of resolution, and 39 ms of exposure time. The Amide software (version 1.0.4) was utilized to obtain the three-dimensional (3-D) reconstructed images of the mouse.

In vivo photodynamic therapy

When tumor volumes reached \sim 50 mm³, 0.2 mL of free or liposomal TPPS₄ in PBS (all the injections contained 0.16 mg·kg⁻¹ TPPS₄) were administered intravenously (tail vein). All mice were randomly divided into no treatment groups and irradiation treatment groups (5 mice in every group). The tumors of the mice in the irradiation groups were irradiated with a 640 nm laser (60 J·cm⁻²) 24 h post injection. After PDT treatment, the tumor volumes and animal weights were measured every three days.

Statistical analysis

The measurement experiments were repeated at least three times. The data were expressed in mean \pm standard error of the mean (SEM) or standard deviation (SD). The statistically significant differences amongst different groups were evaluated by a Student's *t*-test. A *p*-value less than 0.05 was considered significant.

Abbreviations

¹O₂: singlet oxygen; ABDA: 9, 10-Anthracenediyl-bis(methylene)dimalonic acid; CCK-8: Cell Counting Kit-8; CT: computed tomography; CTIA: CT imaging contrast agent; DLS: dynamic light scattering; DMEM: Dulbecco's modified eagle's medium; DMSO: dimethyl sulfoxide; DOTAP: 1,2-dioleoyl-3-trimethylammonium-propane (chloride salt); DPPC: 1,2-dipal-

mitoyl-sn-glycero-3-phosphocholine; DSPE-PEG2000: 1,2-distearoyl-sn-glycero-3-phosphoethanolamine-N-[amino(polyethylene, glycol)-2000] (ammonium salt); FBS: fetal bovine serum; FL: Fluorescence; LIT: NL co-encapsulation of iodixanol and TPPS₄; MEC: molar extinction coefficient; NL: nanoliposomes; PBS: Phosphate-buffered saline; PDI: polydispersity index; PDT: photodynamic therapy; PS: photosensitizer; RMP1 1640: Roswell Park Memorial Institute 1640; ROS: reactive oxygen species; TPPS₄: meso-tetrakis (4-sulphonatophenyl) porphine.

Supplementary Material

Supplementary figures and tables.

<http://www.thno.org/v09p1323s1.pdf>

Acknowledgements

This work has been partially supported by the Basic Research Program of China (2015CB352005), National Natural Science Foundation of China (61705139, 61875135, 61525503, 61620106016, 61835009, 81727804), the Guangdong Natural Science Foundation Innovation Team (2014A030312008, 2017A030310136), Shenzhen Basic Research Project (JCYJ20150930104948169, JCYJ20160328144746940, GJHZ20160226202139185, JCYJ20170412105003520, JCYJ20170817094735945, JCYJ20170818090620324), China Postdoctoral Science Foundation (2017M612724), the University of Macau (MYRG2015-00036-FHS, MYRG2016-00110-FHS, MYRG2018-00081-FHS), and the Macao Science and Technology Development Fund (FDCT 025/2015/A1, FDCT 0011/2018/A1). We thank Instrumental Analysis Center of Shenzhen University (Xili campus) for providing access to TEM.

Author contributions

T.Y.O. and H.X. conceived the study and designed research; H.X., T.Y.O., A.Y., R.Z. performed the experiments; H.X., T.Y.O., J.S., L.L., J.Q., Z.Y. analyzed the results; H.X. and T.Y.O. drafted the manuscript; T.Y.O., J.Q. and Z.Y. supervised the study, edited and finalized the manuscript.

Competing Interests

The authors have declared that no competing interest exists.

References

- Xie J, Lee S, Chen X. Nanoparticle-based theranostic agents. *Adv Drug Deliv Rev.* 2010; 62: 1064-79.
- Lovell JF, Liu TWB, Chen J, Zheng G. Activatable photosensitizers for imaging and therapy. *Chem Rev.* 2010; 110: 2839-57.
- Celli J, Spring B, Rizvi I, Evans CL, Samkoe KS, Verma S, et al. Imaging and photodynamic therapy: mechanisms, monitoring and optimization. *Chem Rev.* 2010; 110: 2795-838.
- Josefsen LB, Boyle RW. Unique diagnostic and therapeutic roles of porphyrins and phthalocyanines in photodynamic therapy, imaging and theranostics. *Theranostics.* 2012; 2: 916-66.
- Rai P, Mallidi S, Zheng X, Rahmanzadeh R, Mir Y, Elrington S, et al. Development and applications of photo-triggered theranostic agents. *Adv Drug Deliv Rev.* 2010; 62: 1094-124.
- Yan X, Niu G, Lin J, Jin AJ, Hu H, Tang Y, et al. Enhanced fluorescence imaging guided photodynamic therapy of sinoporphyrin sodium loaded graphene oxide. *Biomaterials.* 2015; 42: 94-102.
- Fan W, Huang P, Chen X. Overcoming the Achilles' heel of photodynamic therapy. *Chem Soc Rev.* 2016; 45: 6488-519.
- Hasan T, Ortel B, Moor ACE, Pogue BW. Photodynamic therapy of Cancer. In: Kufe DW, Pollock RE, Weichselbaum RR, Robert C Bast J, Gansler TS, Holland JF, et al. Ed. *Holland-Frei Cancer Med*, 6th ed. Hamilton, Canada: B.C. Decker; 2003: 605-22.
- Glidden MD, Celli JP, Massodi I, Rizvi I, Pogue BW, Hasan T. Image-based quantification of benzoporphyrin derivative uptake, localization, and photobleaching in 3D Tumor Models, for optimization of PDT parameters. *Theranostics.* 2012; 2: 827-39.
- Patel N, Pera P, Joshi P, Dukh M, Tabaczynski WA, Sifers KE, et al. Highly effective dual-function near-infrared (NIR) photosensitizer for fluorescence imaging and photodynamic Therapy (PDT) of Cancer. *J Med Chem.* 2016; 59: 9774-87.
- Lucky SS, Soo KC, Zhang Y. Nanoparticles in photodynamic therapy. *Chem Rev.* 2015; 115: 1990-2042.
- Ding J, Wang Y, Ma M, Zhang Y, Lu S, Jiang Y, et al. CT/fluorescence dual-modal nanoemulsion platform for investigating atherosclerotic plaques. *Biomaterials.* 2013; 34: 209-16.
- Kepshire D, Mincu N, Hutchins M, Gruber J, Dehghani H, Hynarowski J, et al. A microcomputed tomography guided fluorescence tomography system for small animal molecular imaging. *Rev Sci Instrum.* 2009; 80: 1-10.
- Ekdawi SN, Stewart JMP, Dunne M, Stapleton S, Mitsakakis N, Dou YN, et al. Spatial and temporal mapping of heterogeneity in liposome uptake and microvascular distribution in an orthotopic tumor xenograft model. *J Control Release.* 2015; 207: 101-11.
- Zhang C, Ren J, Hua J, Xia L, He J, Huo D, et al. Multifunctional Bi₂WO₆ nanoparticles for CT-guided photothermal and oxygen-free photodynamic therapy. *ACS Appl Mater Interfaces.* 2018; 10: 1132-46.
- Chen J, Yang XQ, Meng YZ, Qin MY, Yan DM, Qian Y, et al. Reverse microemulsion-mediated synthesis of Bi₂S₃-QD@SiO₂-PEG for dual modal CT-fluorescence imaging in vitro and in vivo. *Chem Commun.* 2013; 49: 11800-2.
- Luo T, Huang P, Gao G, Shen G, Fu S, Cui D, et al. Mesoporous silica-coated gold nanorods with embedded indocyanine green for dual mode X-ray CT and NIR fluorescence imaging. *Opt Express.* 2011; 19: 17030.
- Oh MH, Lee N, Kim H, Park SP, Piao Y, Lee J, et al. Large-scale synthesis of bioinert tantalum oxide nanoparticles for X-ray computed tomography imaging and bimodal image-guided sentinel lymph node mapping. *J Am Chem Soc.* 2011; 133: 5508-15.
- Lim C, Shin J, Kwon IC, Jeong SY, Kim S. Iodinated photosensitizing chitosan: self-assembly into tumor-homing nanoparticles with enhanced singlet oxygen generation. *Bioconjug Chem.* 2012; 23: 1022-8.
- Obaid G, Broekgaarden M, Bulin A, Huang H, Kuriakose J, Hasan T. Photonanomedicine: a convergence of photodynamic therapy and nanotechnology. *Nanoscale.* 2016; 8: 12471-503.
- D'Mello SR, Cruz CN, Chen ML, Kapoor M, Lee SL, Tyner KM. The evolving landscape of drug products containing nanomaterials in the United States. *Nat Nanotechnol.* 2017; 12: 523-9.
- Ghaghada KB, Badea CT, Karumbaiah L, Fetting N, Bellamkonda R V., Johnson GA, et al. Evaluation of tumor microenvironment in an animal model using a nanoparticle contrast agent in computed tomography imaging. *Acad Radiol.* 2011; 18: 20-30.
- Bechet D, Couleaud P, Frochot C, Viriot ML, Guillemin F, Barberi-Heyob M. Nanoparticles as vehicles for delivery of photodynamic therapy agents. *Trends Biotechnol.* 2008; 26: 612-21.
- Roy I, Ohulchanskyy TY, Pudavar HE, Bergey EJ, Oseroff AR, Morgan J, et al. Ceramic-based nanoparticles entrapping water-insoluble photosensitizing anticancer drugs: A novel drug-carrier system for photodynamic therapy. *J Am Chem Soc.* 2003; 125: 7860-5.
- Verteporfin Roundtable 2000 and 2001 Participants, Treatment of age-related macular degeneration with photodynamic therapy (TAP) study group principal investigators, Verteporfin in photodynamic therapy (VIP) study group principal investigators. Guidelines for using verteporfin (VISUDYNE®) in photodynamic therapy to treat choroidal neovascularization due to age-related macular degeneration and other causes. *Retina.* 2002; 22: 6-8.
- Huang H, Hasan T. The "Nano" world in photodynamic therapy. *Austin J Nanomedicine Nanotechnol.* 2014; 2: 1-4.
- Mallidi S, Spring BQ, Chang S, Vakoc B, Hasan T. Optical Imaging , Photodynamic Therapy and Optically Triggered Combination Treatments. *Cancer J.* 2015; 21: 194-205.
- Spring BQ, Bryan Sears R, Zheng LZ, Mai Z, Watanabe R, Sherwood ME, et al. A photoactivable multi-inhibitor nanoliposome for tumour control and simultaneous inhibition of treatment escape pathways. *Nat Nanotechnol.* 2016; 11: 378-87.
- Jermyn M, Davis SC, Dehghani H, Huggett MT, Hasan T, Pereira SP, et al. CT contrast predicts pancreatic cancer treatment response to verteporfin-based photodynamic therapy. *Phys Med Biol.* 2014; 59: 1911-21.

30. Kobayashi H, Watanabe R, Choyke PL. Improving conventional enhanced permeability and retention (EPR) effects; What is the appropriate target? *Theranostics*. 2014; 4: 81-9.
31. Vemuri S, Rhodes CT. Preparation and characterization of liposomes as therapeutic delivery systems: a review. *Pharm Acta Helv*. 1995; 70: 95-111.
32. Oliveira MF, Guimarães PPG, Gomes ADM, Suárez D, Sinisterra RD. Strategies to target tumors using nanodelivery systems based on biodegradable polymers, aspects of intellectual property, and market. *J Chem Biol*. 2013; 6: 7-23.
33. Derycke ASL, Witte PAM de. Liposomes for photodynamic therapy. *Adv Drug Deliv Rev*. 2004;56: 17-30.
34. Xia Y, Tian J, Chen X. Effect of surface properties on liposomal siRNA delivery. *Biomaterials*. 2016; 79: 56-68.
35. Campbell RB, Balasubramanian S V., Straubinger RM. Phospholipid-cationic lipid interactions: influences on membrane and vesicle properties. *Biochim Biophys Acta*. 2001; 1512: 27-39.
36. Mallidi S, Anbil S, Lee S, Manstein D, Elrington S, Kosiratna G, et al. Photosensitizer fluorescence and singlet oxygen luminescence as dosimetric predictors of topical 5-aminolevulinic acid photodynamic therapy induced clinical erythema. *J Biomed Opt*. 2014; 19: 028001.
37. Xu H, Liu C, Mei J, Yao C, Wang S, Wang J, et al. Effects of light irradiation upon photodynamic therapy based on 5-aminolevulinic acid-gold nanoparticle conjugates in K562 cells via singlet oxygen generation. *Int J Nanomedicine*. 2012; 7: 5029-38.
38. Laubach HJ, Chang SK, Lee S, Rizvi I, Zurakowski D, Davis SJ, et al. In-vivo singlet oxygen dosimetry of clinical 5-aminolevulinic acid photodynamic therapy. *J Biomed Opt*. 2008; 13: 050504.
39. Kim S, Ohulchanskyy TY, Bharali D, Chen Y, Pandey RK, Prasad PN. Organically modified silica nanoparticles with intraparticle heavy-atom effect on the encapsulated photosensitizer for enhanced efficacy of photodynamic therapy. *J Phys Chem C*. 2009; 113: 12641-4.
40. Ohulchanskyy TY, Roy I, Goswami LN, Chen Y, Bergey EJ, Pandey RK, et al. Organically modified silica nanoparticles with covalently incorporated photosensitizer for photodynamic therapy of cancer. *Nano Lett*. 2007; 7: 2835-42.
41. Kim S, Ohulchanskyy TY, Pudavar HE, Pandey RK, Prasad PN. Organically modified silica nanoparticles co-encapsulating photosensitizing drug and aggregation-enhanced two-photon absorbing fluorescent dye aggregates for two-photon photodynamic therapy. *J Am Chem Soc*. 2007; 129: 2669-75.
42. Kuznetsova NA, Gretsova NS, Yuzhakova OA, Negrimovskii VM, Kaliya OL, Luk'yanets EA. New reagents for determination of the quantum efficiency of singlet oxygen generation in aqueous media. *Russ J Gen Chem*. 2001; 71: 36-41.
43. Ohulchanskyy TY, Donnelly DJ, Detty MR, Prasad PN. Heteroatom substitution induced changes in excited-state photophysics and singlet oxygen generation in chalcogenoxanthylum dyes: Effect of sulfur and selenium substitutions. *J Phys Chem B*. 2004; 108: 8668-72.
44. Kryman MW, Schamerhorn GA, Yung K, Sathyamoorthy B, Sukumaran DK, Ohulchanskyy TY, et al. Organotellurium fluorescence probes for redox reactions: 9-aryl-3,6-diaminotelluroxanthylum dyes and their telluroxides. *Organometallics*. 2013; 32: 4321-33.
45. Lim CK, Shin J, Lee YD, Kim J, Park H, Kwon IC, et al. Heavy-atomic construction of photosensitizer nanoparticles for enhanced photodynamic therapy of cancer. *Small*. 2011; 7: 112-8.
46. Grebenová D, Cajthamlová H, Holada K, Marinov J, Jirsa M, Hrkal Z. Photodynamic effects of meso-tetra (4-sulfonatophenyl)porphine on human leukemia cells HEL and HL60, human lymphocytes and bone marrow progenitor cells. *J Photochem Photobiol B*. 1997; 39: 269-78.
47. Strauss WSL, Gschwend MH, Sailer R, Schneckenburger H, Steiner R, Rück A. Intracellular fluorescence behaviour of meso-tetra(4-sulfonatophenyl) porphyrin during photodynamic treatment at various growth phases of cultured cells. *J Photochem Photobiol B Biol*. 1995; 28: 155-61.
48. Gabizon A, Catane R, Uziely B, Kaufman B, Safra T, Cohen R, et al. Prolonged circulating time and enhanced accumulation in malignant exudates of doxorubicin encapsulated in polyethylene- glycol coated liposomes. *Cancer Res*. 1994; 54: 987-92.
49. Barenholz Y. Doxil® - The first FDA-approved nano-drug: Lessons learned. *J Control Release*. 2012; 160: 117-34.
50. Ježek P, Nekvasil M, Škobisová E, Urbánková E, Jirsa M, Zadinová M, et al. Experimental photodynamic therapy with meso-tetrakisphenylporphyrin (TPP) in liposomes leads to disintegration of human amelanotic melanoma implanted to nude mice. *Int J Cancer*. 2003; 103: 693-702.
51. Choi D, Jeon S, You DG, Um W, Kim J, Yoon HY. Iodinated echogenic glycol chitosan nanoparticles for X-ray CT/US dual imaging of tumor. *Nanotheranostics*. 2018; 2: 117-27.
52. Hayashi K, Nakamura M, Miki H, Ozaki S, Abe M, Matsumoto T, et al. Photostable iodinated silica/porphyrin hybrid nanoparticles with heavy-atom effect for wide-field photodynamic/photothermal therapy using single light source. *Adv Funct Mater*. 2014; 24: 503-13.
53. Dong C, Liu Z, Wang S, Zheng B, Guo W, Yang W, et al. A protein-polymer bioconjugate-coated upconversion nanosystem for simultaneous tumor cell imaging, photodynamic therapy and chemotherapy. *ACS Appl Mater Interfaces*. 2016; 8: 32688-98.
54. Tominaga H, Ishiyama M, Ohseto F, Sasamoto K, Hamamoto T, Suzuki K, et al. A water-soluble tetrazolium salt useful for colorimetric cell viability assay. *Anal Commun*. 1999; 36: 47-50.